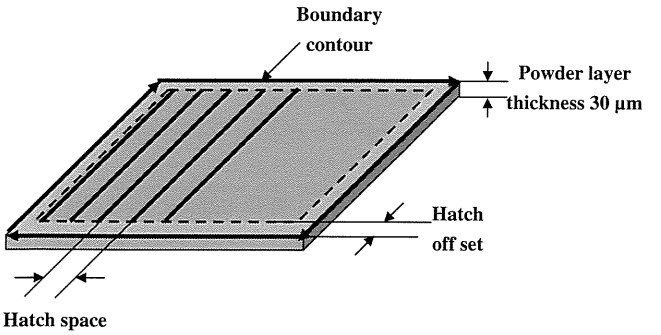

Fig. 2. Schematic representation of various operating parameters which affect the product density in the SLM process.

Therefore, a foothold was provided for the bone structure. Then the image was sliced at 30 μm intervals. Porous structures were fabricated using Ti metal powder according to the sliced data by the method described in Section 2.2.1. Fig. 3a shows a CT image of the cancellous bone structure of a 53-year-old male, while (i) is a porous body produced by multiple stacking of the unit structure in (a). Fig. 3b shows a CT image of the cancellous bone of a 48-year-old female, while (ii) is a porous body produced from (b). Fig. 3ii is referred to as CBS in subsequent studies. Fig. 3c shows a hollow cubic unit cell and its stacking, while (iii) is a porous body produced from (c). This is referred to as IPS in subsequent studies. These three types of specimens were produced with different porosities by changing the wall thickness. Cancellous bone structures consist of interconnected pores of different sizes ranging from 500 μm to 2 mm (Fig. 3i and ii), while the cubic structure has interconnected pores in the range 400–800 μm (Fig. 3iii). These specimens were washed with acetone, 2-propanol, and ultrapure water for 30 min each in an ultrasonic cleaner and then dried in an oven at 40 °C overnight. Later, the CBS and IPS specimens were subjected to heat treatment at 1300 °C in an argon gas atmosphere to smooth the surface.

2.3. Chemical and heat treatment for bioactivity

The porous Ti metal specimens CBS and IPS were first soaked in 5 M NaOH solution at 60 °C for 24 h and then soaked in 0.5 mM HCl solution at 40 °C for 3 h to bioactivate them. A continuous-flow method was used to treat these specimens to avoid non-uniform chemical treatment inside the pores along the length. Later, these specimens were washed in ultrapure water, dried in an oven at 40 °C overnight and then heated to 600 °C at a rate of 5 °C min^{-1}. The specimens were kept in a Fe–Cr electric furnace under an air atmosphere at 600 °C for 1 h and finally cooled to room temperature naturally in the furnace.

2.4. Analysis of the surface structures and measurement of compressive strength

The surface texture of the porous Ti metal as prepared, in addition to being subsequently subjected to heat treatment at 1300 °C in an argon gas atmosphere, was observed by field emission scanning electron microscopy (FE-SEM) (Hitachi S-4300, Japan). Surface structural changes due to the NaOH, HCl, and heat treatments and subsequent soaking in SBF were also observed by FE-SEM.

The compressive strengths of porous bodies of Ti metal with the different structures shown in Fig. 3i–iii were measured using a universal testing machine (model EHF-LV020K1-010, Shimadzu Corp., Japan) at a cross-head speed of 1 mm min^{-1}.

2.5. Examination of the apatite forming ability in a simulated body fluid (SBF)

Porous Ti metal subjected to chemical and heat treatment was soaked in 30 ml of an acellular SBF with ion concentrations of Na^+ 142.0, K^+ 5.0, Mg^{2+} 1.5, Ca^{2+} 2.5, Cl^-147.8, HCO_3^- 4.2, HPO_4^{2-} 1.0, and SO_4^{2-} 0.5 mM, nearly equal to those of human blood plasma, at 36.5 °C for 3 days. The SBF was prepared by dissolving reagent grade NaCl, $NaHCO_3$, KCl, $K_2HPO_4{\cdot}3H_2O$, $MgCl_2{\cdot}6H_2O$, $CaCl_2$, and Na_2SO_4 (Nacalai Tesque Inc., Kyoto, Japan) in ultrapure

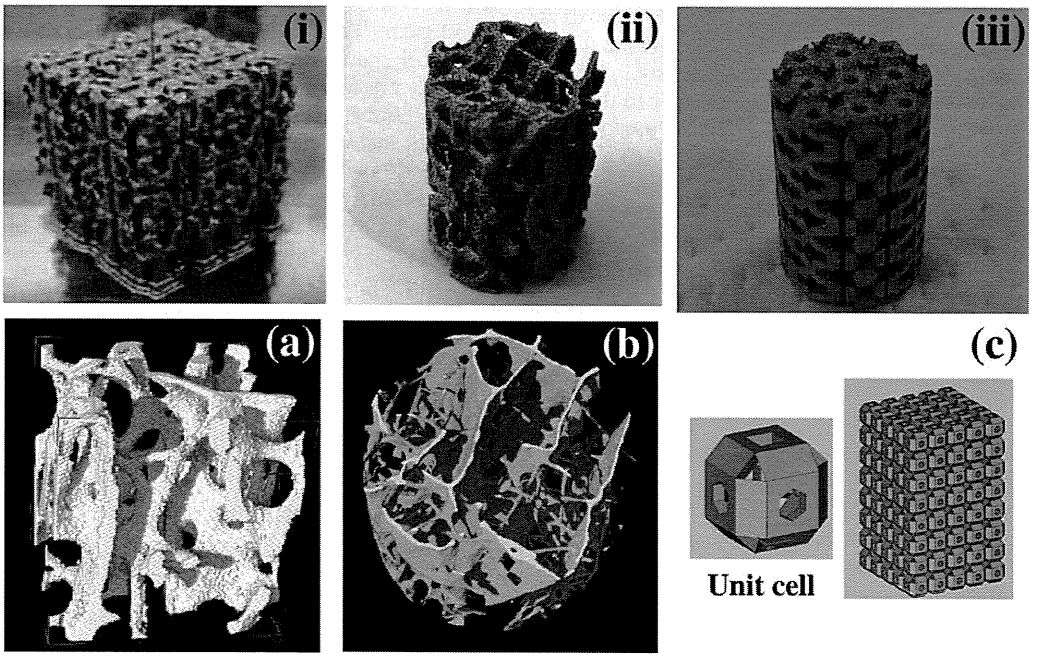

Fig. 3. Titanium porous structure fabricated by SLM (i–iii) based on micro-CT images of human cancellous bones (a, b) and stacked hollow cubes (c). Specimen size: (a) 15 × 15 × 15 mm; (b, c) 6 mm diameter, 10 mm length. Notation: (ii) CBS; (iii) IPS.

water buffered at pH 7.40 with Tris and 1 M HCl (Nacalai Tesque) [29]. After 3 days soaking the specimens were removed from the SBF, gently washed with ultrapure water, and dried at 40 °C in an oven. Apatite formation on the walls was examined by FE-SEM.

2.6. In vivo examination of new bone formation in white rabbits

2.6.1. Animal study

Porous Ti metal specimens of CBS and IPS 6 mm in outer diameter and 15 mm in length, subjected to chemical and heat treatments, were conventionally sterilized using ethylene oxide gas and implanted into the metaphyses of the femoral condyles of mature male Japanese white rabbits weighing 2.8–3.5 kg. The surgical methods used have been described elsewhere [30,31]. Briefly, the rabbits were anesthetized with intravenous injections of sodium pentobarbital (0.5 ml kg^{-1}), an intramuscular injection of ketamine hydrochloride (10 mg kg^{-1}), and local administration of a solution of 1% lidocaine. After shaving, disinfection, and draping, the fascia was split and a 6 mm diameter drill hole was made through the femoral condyles. After irrigating the hole with saline, both kinds of porous Ti metal specimens, CBS and IPS, subjected to chemical and heat treatment, were implanted into the hole. For comparison, untreated samples were also implanted in a similar manner. Surgical procedures were performed bilaterally. Twenty-five rabbits were used for the chemical- and heat-treated implants. At 3, 6, 12, 26, and 52 weeks after implantation five rabbits were killed using an overdose of intravenous sodium pentobarbital, i.e. five chemical- and heat-treated implants and five animals per experimental condition. Ten rabbits were used for the untreated implants. At 12 and 52 weeks after implantation these rabbits were killed in the same way, i.e. five untreated implants and five animals per experimental condition. This animal study was approved by the Animal Research Committee, Graduate School of Medicine, Kyoto University, Japan.

2.6.2. Histological examination

Following death the implant sites were removed and prepared for histology. The specimens were fixed in 10% phosphate-buffered formalin, pH 7.25 for 7 days and dehydrated in serial concentrations of ethanol (70%, 80%, 90%, 99%, 100%, and 100% v/v) for 3 days each. Specimens were then embedded in polyester resin. Thick sections (250 μm) were cut with a band saw (BS-3000CP, EXACT Cutting Systems, Norderstedt, Germany) perpendicular to the axis of the implant and ground to a thickness of 50–60 μm using a grinding–sliding machine (Microgrinding MG-4000, EXACT Cutting Systems). Each section was then stained with Stevenel's blue and Van Gieson's picrofuchsin [32]. A thorough microscopic analysis was performed on histological slides using transmitted light microscopy (model Eclipse 80i, Nikon Co., Japan) combined with a digital camera (model DS-5 M-L1, Nikon Co., Japan).

Other thick sections (500 μm) were cut with a band saw, polished with diamond paper, and a thin layer of carbon applied for observation by SEM.

2.6.3. Histomorphometric examination

The bone affinity index (%) was measured on a personal computer using Adobe Photoshop CS3 and Image J (NIH) for each implant using data provided by light microscopy and fluorescence microscopy. The bone affinity index is defined as the fraction of bone contact over the entire wall of the pores in the implant [26,31,33]. Two sections surrounded with cancellous bone from either the medial or the lateral condyles were examined for each implant. Thus, 10 slices were analyzed for each implantation time.

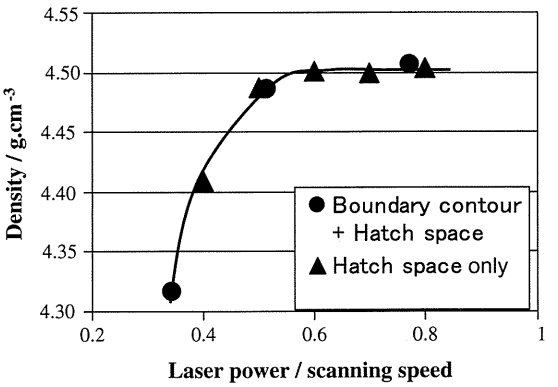

Fig. 4. Variation in density of the solid cubic specimens with change in laser power to scanning speed ratio at a constant powder layer thickness. Specimen size 9 × 9 × 9 mm^3; hatch space 180 μm; scanning speed 225 mm s^{-1}.

2.6.4. Statistical analysis

All data are expressed as means ± standard deviation (SD) and were statistically analyzed using JMP IN 5.1 (SAS Institute, Cary, NC). The unpaired one-tailed Student's *t*-test was used for comparison between the implant (bioactive treated and untreated) at each time point (12 and 52 weeks). One-way ANOVA followed by post hoc tests (Tukey–Kramer multiple comparison tests) were used to analyze temporal bone formation in each implant type. Differences at $P < 0.05$ were considered statistically significant.

3. Results

3.1. Effects of processing parameters on the density of the specimen

Fig. 4 shows the variation in density of specimens with laser power to scanning speed (*P*/*V*) ratio, where specimens were fabricated using a boundary contour followed by a hatch beam with a hatch space of 180 μm. Specimens were also prepared using only a hatch beam with a hatch space of 180 μm. From Fig. 4 we can see that in both cases the density of the specimen was low when the *P*/*V* ratio was <0.5, and reached the theoretical density (4.51 g cm^{-3}) of Ti metal when the P/V ratio was >0.60.

Fig. 5 shows the density of Ti plates of different thicknesses, which were fabricated at two different hatch beam spaces of 90 and 180 μm at a constant *P*/*V* ratio of 0.51. The density was nearly equal to that of the theoretical density when the thickness of the prepared specimen was >1.8 mm, irrespective of the space between the two consecutive hatch beams. A high density was observed for plates with a thickness of <1.8 mm when the hatch beam space was 90 μm. The effect of hatch beam offsets of 0, 10,

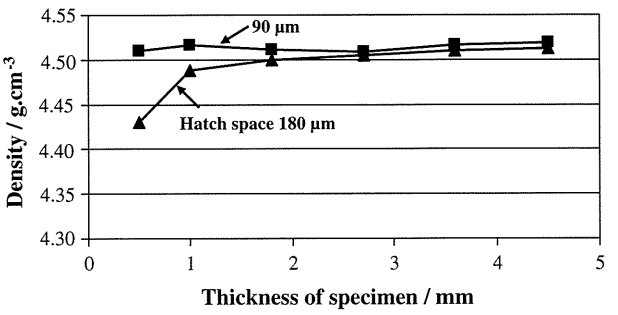

Fig. 5. Effect of hatch space on density of solid specimens of different thicknesses. Specimen size 9 × 9 × *t* mm^3, where *t* is the thickness of specimen in mm; scanning speed 225 mm s^{-1}.

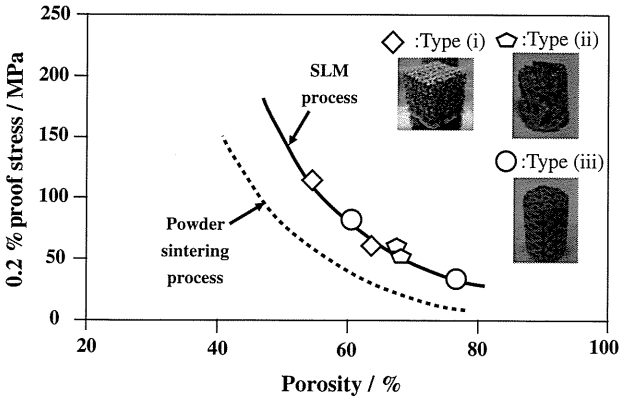

Fig. 6. Compressive strength of porous Ti metal with respect to porosity prepared by selective laser melting and compared with those prepared by a conventional powder sintering process.

and 20 μm on the density of the specimens was also examined, and the results showed similar densities of the final products in all cases.

Based on these results, a laser power of 117 W, scanning speed of 225 mm s^{-1}, hatch space of 90 μm, and hatch offset of 20 μm were used to fabricate porous bodies with a wall thickness of <1.8 mm.

3.2. Compressive strength of the porous specimens

The wall thicknesses of the various types of fabricated porous structures shown in Fig. 3 were in the range 400–800 μm. Cancellous bone structures consist of pores of different sizes ranging from 500 μm to 2 mm (Fig. 3i and ii), while the cubic structure has pores in the range 400–800 μm (Fig. 3iii). The compressive strengths of the various kinds of porous Ti metal fabricated by the SLM process is plotted against porosity in Fig. 6. The compressive strength was in the range 35–120 MPa when the porosities were in the range 75–55%. The results were compared with those of porous Ti metal prepared by the powder sintering method. The compressive strength of porous specimens fabricated by SLM was higher than that of those prepared by powder sintering, while the strength of specimens generated by both methods decreased with increasing porosity [3].

3.3. Surface structural changes on heat treatment

Fig. 7 shows the surface texture of the fabricated specimen, as well as of that subjected to heat treatment at 1300 °C in an argon gas atmosphere. Partially melted Ti particles were loosely bonded to the surface of the fabricated specimen. However, after heat treatment at 1300 °C, these particles were fused and bonded with the laser melted core part, producing a concave texture over the entire surface.

3.4. Surface structural changes in porous Ti metal on chemical and heat treatment and soaking in SBF

Fig. 8 shows FE-SEM photographs of a porous Ti metal that had been subjected to chemical and heat treatment after heat treatment at 1300 °C in an argon gas atmosphere. A fine network structure was formed on the surface of the porous Ti metal. These network structures were uniformly observed, even on the inner side of the pore.

Fig. 9 shows FE-SEM photographs of porous Ti metal soaked in SBF for 3 days after chemical and heat treatment. The walls of the porous body were completely covered with apatite after soaking in SBF for 3 days, indicating that the Ti metal surface had become bioactive after NaOH, HCl, and heat treatment.

3.5. In vivo bioactivity of the porous Ti metal

Gross inspection of the animal experiments showed that all rabbits tolerated the operative procedure well. No infection of the

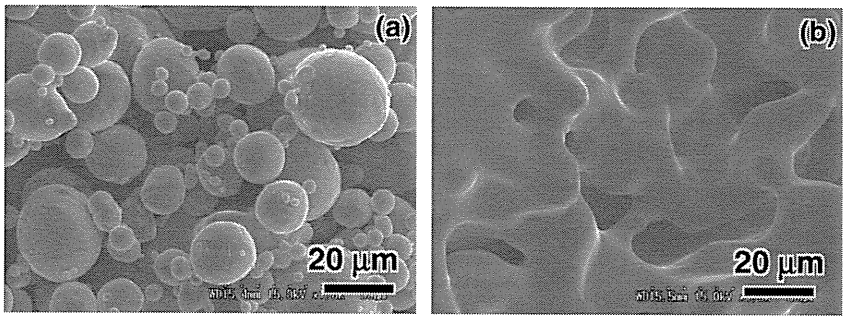

Fig. 7. FE-SEM photograph of the surface of porous Ti metal CBS (a) fabricated by SLM and (b) that heated at 1300 °C for 1 h in an argon gas atmosphere.

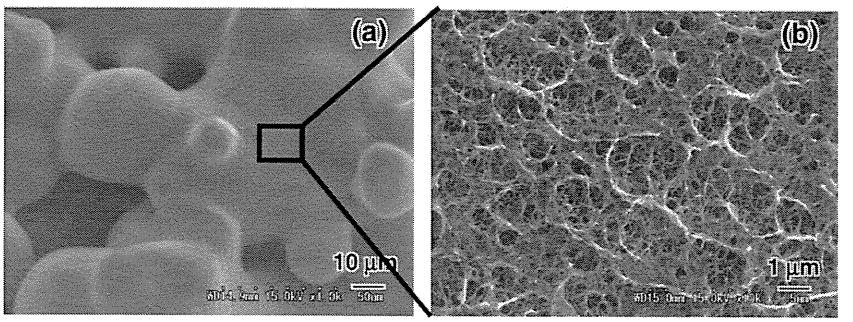

Fig. 8. FE-SEM photograph of porous Ti metal CBS subjected to NaOH, HCl and heat treatments after heat treatment at 1300 °C. (a) Low magnification; (b) high magnification showing fine network structure on the wall.

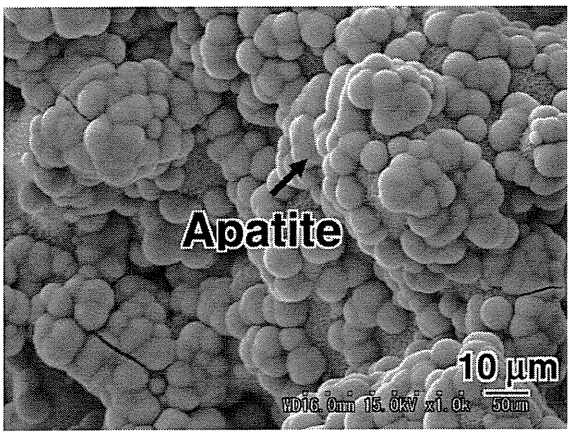

Fig. 9. Apatite particles formed on the surface of porous Ti metal CBS soaked in SBF for 3 days after NaOH, HCl and heat treatments.

operative site or dislocations of the implants were observed on dissection after death. All implanted porous Ti metal CBS and IPS specimens were stable and firmly bonded with the host bone at all post-implantation time points. No apparent adverse reactions, such as inflammation or foreign body reactions, were noted on or around any implanted samples by Stevenel's blue and Van Gieson's surface staining.

Within 3 weeks new bone was observed at the outer periphery and in the center of the chemical- and heat-treated specimens (results not shown). At the advancing bone front in the deep portion of the sample immature woven bone was found. There was no sign of cartilage formation or endochondral ossification. Marrow-like tissue formation was observed in the samples. Fig. 10 shows light microscope and SEM photographs of chemical- and heat-treated and untreated CBS samples 12 weeks after implantation. From Fig. 10 we can see that new bone was formed on the porous surface and bonded directly with the chemically treated layer. On the other hand, little new bone formation was observed on the surface of untreated implants. Fig. 11 shows a comparative histological study of porous Ti metal CBS and IPS samples subjected to chemical and heat treatment and implanted into the femurs of rabbits for 12 weeks. From Fig. 11 we can see that both CBS and IPS specimens showed mature bone strongly adhering to the porous wall. Fig. 12 shows the bone affinity indices (%) for chemical- and heat-treated CBS and IPS samples as well as for untreated samples for different implantation periods. The affinity indices of chemical- and heat-treated porous Ti metal CBS and IPS samples gradually increased with implantation period. There was a significant difference between the 52 week period and the other periods for the chemical- and heat-treated porous Ti metal CBS and IPS samples. After 12 and 52 weeks implantation the affinity indices of chemical- and heat-treated implants were significantly greater than those of the untreated implants.

4. Discussion

Using conventional fabrication techniques it is difficult to control the internal pore geometry, pore size, and distribution [3,34]. On the other hand, the SLM process is a useful technique to fabricate 3D porous structures directly from metallic powders and, hence, the process is suitable for the design of artificial bone substitutes with complex inner and outer geometries fitting the patient's defective bone. However, in this technique fine metal powders are melted by laser beam, which moves at a very high speed, and hence, this melting process may create internal defects due to some of the powder being blown off. In order to fabricate defect-free metallic implants it is important to optimize the power, scanning speed, and scanning pattern of the laser beam.

When the supplied energy density is insufficient to fully melt the powder, unmelted powder remains on the layer and produces defects. The temperature of the powder in the vicinity of the melted zone is low. In contrast, when the supplied energy density is sufficient to melt the powder, the melting zone becomes large and the temperature in the vicinity of the melted zone will remain high. This high temperature assists full melting of the powder in the next layer. Therefore, the density of the specimen depends

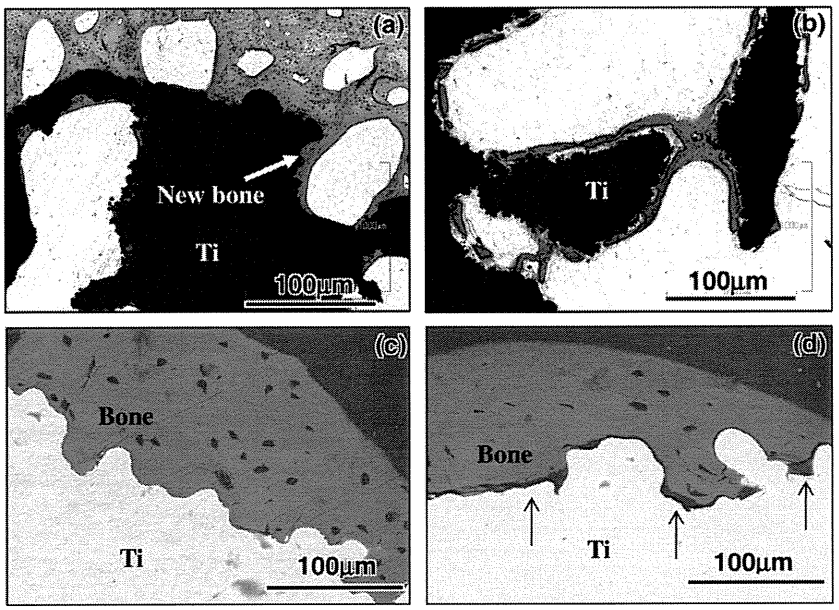

Fig. 10. Stevenel's blue and Van Gieson's surface staining of non-decalcified histological sections and SEM photographs of CBS samples after 12 weeks implantation. (a, c) Chemical- and heat-treated implants show new bone formation along the pore walls; (b, d) untreated implants show slight new bone formation along the pore walls. Red indicates bone. (For interpretation of the references to colour in this figure legend, the reader is referred to the web version of this article).

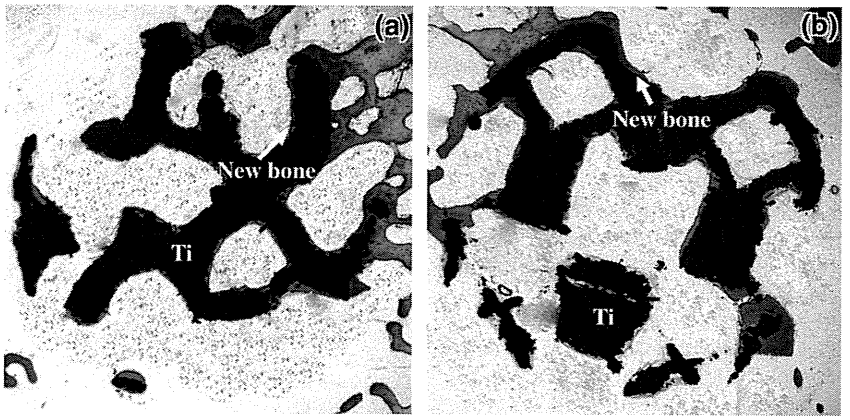

Fig. 11. Stevenel's blue and van Gieson's surface staining of non-decalcified histological section of chemical- and heat-treated porous Ti implants CBS and IPS after 12 weeks implantation in the femur of white rabbits.

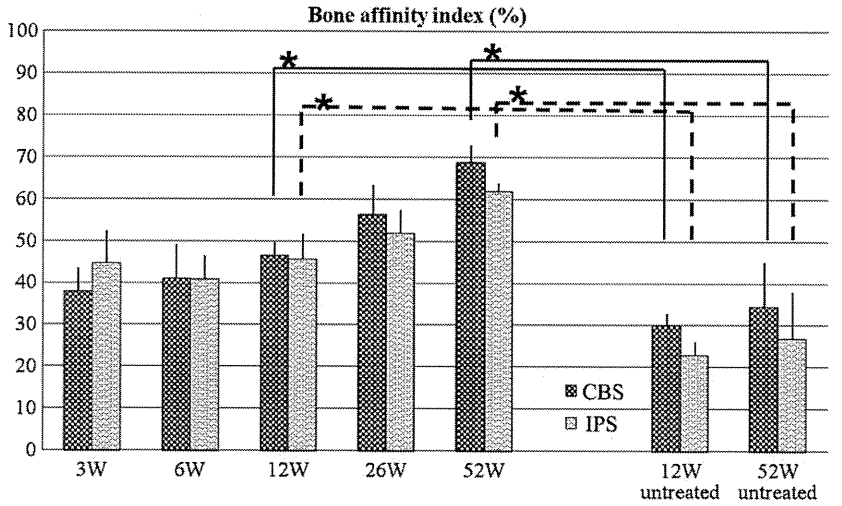

Fig. 12. Affinity indices (%) of the chemical- and heat-treated porous Ti implants CBS and IPS implanted in the femur of rabbit for different durations. The error bars are standard deviations. * Significant difference.

on the supplied energy density or on the ratio of laser power to scanning speed (P/V) at a constant thickness of powder layer. The critical value of P/V is approximately 0.5–0.6, as shown in Fig. 4. In general, both a boundary contour and a hatch beam are necessary to give an accurate shape and high density to the final product. However, similar trends in density as a function of P/V were observed when the specimens were fabricated using only a hatch beam, as shown in Fig. 4. As indicated in Fig. 5, the density of the thick plate specimen (>1.8 mm) does not depend on two consecutive hatch spaces. However, a large number of defects remained in the formed body when thin plate specimens (thinner than 1 mm) were fabricated with a hatch spacing of 180 μm, and their densities were low. A fully dense body with a thinner wall measuring 0.5 mm could be prepared by decreasing the space between the two consecutive hatch beams to 90 μm, as shown in Fig. 5. This suggests that two consecutive beams should be overlapped to fabricate thinner walls. When a laser beam scans to melt the powders to form a thin wall, the temperature is easily reduced by thermal conduction into the surrounding powder because of its small thermal capacity. This induces insufficient melting of the powder and the formation of internal defects. In the case of the fabrication of thick walls, the laser power is supplied over a wide zone, so the powder surrounding the melt zone remains hot for a longer time, which helps in melting of the Ti powder to reduce the defects and increase the density. If the hatch beam scanning interval is further reduced, defect formation can be avoided, because the energy supplied to the powder for each unit volume is sufficient to keep the temperature high in the melt zone.

In the present study we observed that large numbers of spherical Ti particles were partially bonded to the porous walls. In order to avoid release of these particles, the specimens were heated at 1300 °C in an argon gas atmosphere (Fig. 7). Although the mechanical strength might be decreased by the heat treatment [35], microcavities were formed on the wall, and these might be beneficial for interlock with the surrounding tissues when implanted in the living body. The compressive strength of the porous body processed by SLM was in the range 35–120 MPa when the volumetric porosities were in the range 75–55%. These values are higher than those of porous bodies prepared by the powder sintering method, as seen in Fig. 6. The improved compressive strength is attributed to the fine grain structure formed by rapid cooling of the laser melted body, whereas grain growth occurs during powder sintering. Further, the compressive strength of the porous body prepared by SLM might be little increased by the subsequent chemical and heat treatments [3].

Porous bodies prepared by the SLM process formed a fine uniform network structure on their pore walls after NaOH treatment, and these network structures remained stable even after subse-

quent HCl and heat treatment, as shown in Fig. 8. These network structures, as reported earlier, consist of anatase and rutile [25]. Chemical treatment has the advantage of uniform treatment, even within the pore. Porous bodies subjected to this chemical and heat treatment formed bone-like apatite on soaking in SBF within 3 days, as seen in Fig. 9. It has been believed that if a material forms a bone-like apatite layer on its surface in SBF it can induce direct bone formation through a similar apatite layer in the living body and bond to living bone [21,22]. In the present study similar results were verified in the animal experiments. As shown in Fig. 11, newly formed bone was observed on the periphery and in the center of both kinds of porous structures, CBS and IPS, within 12 weeks after implantation into the femurs of white rabbits. Porous CBS implants showed new bone formation (Fig. 10) in pores and bonded to the wall having nano-structured fine network structures due to previous NaOH, HCl, and heat treatments. On the other hand, untreated implants showed little bone formation in the pores. The amount of new bone on the surface of the untreated implants barely increased with time.

New bone on the surface of chemical- and heat-treated porous Ti metal CBS and IPS gradually increased with implantation time, compared with the untreated porous samples (Fig. 12). This indicates that the porous Ti metal fabricated by the SLM process has a high osteoconductive ability after subsequent NaOH, HCl, and heat treatments, the same as that of plasma sprayed porous Ti metal, as reported earlier [26,36]. Further detailed investigations on the influence of the porous structure on bone growth is in progress, and will be reported elsewhere.

The present study has shown that a porous structure consisting of thin-walled titanium metal with a structure similar to that of human cancellous bone could be prepared by the SLM process by optimizing the laser power, scanning speed, and hatching pattern. This SLM process could be useful to fabricate custom-made implants for biomedical applications tailored to the patient. Internal structure and porosity level can be easily controlled by the automated manufacturing process and, further, bioactivity can be provided by the subsequent chemical and heat treatments.

5. Conclusion

In order to fabricate a porous Ti metal with fully dense thin walls by a SLM process, laser power, scanning speed, and hatching pattern were optimized and various kind of porous bodies were fabricated. The compressive strength of the porous bodies prepared by SLM was found to be higher than that of a powder sintering process at the same level of porosity. Thus, the prepared porous structures analogous to human cancellous bone, when subjected to chemical and heat treatments, uniformly formed a fine network structure of titanium oxide layer, which formed bone-like apatite in SBF within 3 days. In vivo studies showed that newly formed bone was observed in the periphery and in the center of the chemical- and heat-treated cylindrical porous body within 12 weeks of implantation into the rabbit femoral condyle, and was directly bonded to the titanium wall. The SLM process has been found to be a useful technique for fabricating customized metallic implants with complicated internal structures, and the porous bodies thus fabricated are expected to be a useful bone substitutes after chemical and heat treatments.

Appendix A. Figures with essential colour discrimination

Certain figures in this article, particularly Figures 1–3, 6, 10 and 11 are difficult to interpret in black and white. The full colour images can be found in the on-line version, at doi:10.1016/j.actbio.2010.09.034.

References

[1] Ryan G, Pandit A, Apatsidis DP. Fabrication methods of porous metals for use in orthopaedic applications. Biomaterials 2006;27:2651–70.
[2] Wen CE, Yamada Y, Shimojima K, Chino Y, Hosokawa H, Mabuchi M. Novel titanium foam for bone tissue engineering. J Mater Res 2002;17:2633–9.
[3] Pattanayak DK, Matsushita T, Doi K, Takadama H, Nakamura T, Kokubo T. Effects of oxygen content of porous titanium metal on its apatite-forming ability and compressive strength. J Mater Sci Eng C 2009;29:1974–8.
[4] Das S, Wohlert M, Beaman JJ, Bourell DL. Processing of titanium net shapes by SLS/HIP. Mater Des 1999;20:115–21.
[5] Fischer P, Romano V, Weber HP, Karapatis NP, Boillat E, Glardon R. Sintering of commercially pure titanium powder with a Nd:YAG laser source. Acta Mater 2003;51:1651–62.
[6] Simchi A, Petzoldt F, Pohl H. On the development of direct metal laser sintering for rapid tooling. J. Mater Process Technol 2003;141:319–28.
[7] Williams JM et al. Bone tissue engineering using polycaprolactone scaffolds fabricated via selective laser sintering. Biomaterials 2005;26:4817–27.
[8] Santos EC, Shiomi M, Osakada K, Laoui T. Rapid manufacturing of metal components by laser forming. Int J Machine Tools Manuf 2006;46:1459–68.
[9] Traini T, Mangano C, Sammons RL, Mangano F, Macchi A, Piattelli A. Direct laser metal sintering as a new approach to fabrication of an isoelastic functionally graded material for manufacture of porous titanium dental implants. Dent Mater 2008;24:1525–33.
[10] Kumar S, Kruth JP. Composites by rapid prototyping technology. Mater Des 2010;31:850–6.
[11] Hollander DA, Walter MV, Wirtz T, Sellei R, Rohlfing BS, Paar O, et al. Structural, mechanical and in vitro characterization of individually structured Ti6Al4V produced by direct laser forming. Biomaterials 2006;27:955–63.
[12] Lin CY, Wirtz T, LaMarca F, Hollister SJ. Structural and mechanical evaluations of a topology optimized titanium interbody fusion cage fabricated by selective laser melting process. J Biomed Mater Res A 2007;83:272–9.
[13] Yadroitsev I. Bertrand Ph, Smurov I. Parametric analysis of the selective laser melting process. Appl Surf Sci 2007;253:8064–9.
[14] Mullen L, Stamp RC, Brooks WK, Jones E, Sutcliffe CJ. Selective laser melting: a regular unit cell approach for the manufacture of porous, titanium, bone ingrowth constructs, suitable for orthopedic applications. J Biomed Mater Res B Appl Biomater 2009;89:325–34.
[15] Mullen L, Stamp RC, Fox P, Jones E, Ngo C, Sutcliffe CJ. Selective laser melting: a unit cell approach for the manufacture of porous, titanium, bone in-growth constructs, suitable for orthopedic applications. II. Randomized structures. J Biomed Mater Res B Appl Biomater 2009;92:178–88.
[16] Hao L, Dadbakhsh S, Seaman O, Felstead M. Selective laser melting of a stainless steel and hydroxyapatite composite for load-bearing implant development. J Mater Process Technol 2009;209:5793–801.
[17] Stamp R, Fox P, Neill WO, Jones E, Sutcliffe C. The development of a scanning strategy for the manufacture of porous biomaterials by selective laser melting. J Mater Sci Mater Med 2009;20:1839–48.
[18] Thijs L, Verhaeghe F, Craeghs T, Humbeeck JV, Kruth JP. A study of the microstructural evolution during selective laser melting of Ti6Al4V. Acta Mater 2010;58:3303–12.
[19] Heinl P, Muller L, Korner C, Singer RF, Muller FA. Cellular Ti–6Al–4V structures with interconnected macro porosity for bone implants fabricated by selective electron beam melting. Acta Biomater 2008;4:1536–44.
[20] Hacking SA, Tanzer M, Harvey EJ, Krygier JJ, Bobyn JD. Relative contributions of chemistry and topography to the osseointegration of hydroxyapatite coatings. Clin Orthoped Rel Res 2002;405:24–38.
[21] Kim HM, Miyaji F, Kokubo T, Nakamura T. Preparation of bioactive Ti and its alloys via simple chemical surface treatment. J Biomed Mater Res 1996;32:409–17.
[22] Nishiguchi S, Fujibayashi S, Kim HM, Kokubo T, Nakamura T. Biology of alkali- and heat-treated titanium implants. J Biomed Mater Res A 2003;67:26–35.
[23] Fujibayashi S, Neo M, Kim HM, Kokubo T, Nakamura T. Osteoinduction of porous bioactive titanium metal. Biomaterials 2004;25:443–50.
[24] Kawanabe K et al. A new cementless total hip arthroplasty with bioactive titanium porous coating by alkaline and heat treatment: average 4.8 year results. J Biomed Mater Res B Appl Biomater 2009;90:476–81.
[25] Pattanayak DK, Kawai T, Matsushita T, Takadama H, Nakamura T, Kokubo T. Effect of HCl concentrations on apatite-forming ability of NaOH–HCl- and heat-treated titanium metal. J Mater Sci Mater Med 2009;20:1401–11.
[26] Takemoto M, Fujibayashi S, Neo M, Suzuki J, Kokubo T, Nakamura T. Mechanical properties and osteoconductivity of porous bioactive titanium. Biomaterials 2005;26:6014–23.
[27] Takemoto M, Fujibayashi S, Neo M, Suzuki J, Matsushita T, Kokubo T, et al. Osteoinductive porous titanium implants: effect of sodium removal by dilute HCl treatment. Biomaterials 2006;27:2682–91.
[28] Takemoto M et al. A porous bioactive titanium implant for spinal interbody fusion: an experimental study using a canine model. J Neurosur Spine 2007;7:435–43.
[29] Kokubo T, Takadama H. How useful is SBF in predicting in vivo bone bioactivity? Biomaterials 2006;27:2907–15.

[30] Fujibayashi S, Nakamura T, Nishiguchi S, Tamura J, Uchida M, Kim HM, et al. Bioactive titanium: effect of sodium removal on the bone-bonding ability of bioactive titanium prepared by alkali and heat treatment. J Biomed Mater Res 2001;56:562–70.
[31] Fujibayashi S, Neo M, Kim HM, Kokubo T, Nakamura T. A comparative study between in vivo bone ingrowth and in vitro apatite formation on Na_2O–CaO–SiO_2 glasses. Biomaterials 2003;24:1349–56.
[32] Maniatopoulos C, Rodriguez A, Deporter DA, Melcher AH. An improved method for preparing histological sections of metallic implants. Int J Oral Maxillofac Implants 1986;1:31–7.
[33] Nakamura T, Takemoto M. Osteoconduction and its evaluation. In: Kokubo T, editor. Bioceramics and their clinical applications. Cambridge: Woodhead Publishing; 2008. p. 183–98.
[34] Yang YZ, Tian JM, Tian JT, Chen ZQ, Deng XJ, Zhang DH. Preparation of graded porous titanium coatings on titanium implant materials by plasma spraying. J Biomed Mater Res 2000;52:333–7.
[35] Pattanayak DK et al. Fabrication of bioactive porous Ti metal with structure similar to human cancellous bone by selective laser melting. Bioceramics 2009;22:163–6.
[36] Tanaka K, Takemoto M, Fujibayashi S, Kawanabe K, Matsushita T, Kokubo T, et al. Long-term study of osteoconductivity of bioactive porous titanium metals: effect of sodium removal by dilute HCl treatment. Key Eng Mater 2009;396–398:353–6.

Eur Spine J
DOI 10.1007/s00586-011-1728-3

ORIGINAL ARTICLE

A novel synthetic material for spinal fusion: a prospective clinical trial of porous bioactive titanium metal for lumbar interbody fusion

Shunsuke Fujibayashi · Mitsuru Takemoto · Masashi Neo · Tomiharu Matsushita · Tadashi Kokubo · Kenji Doi · Tatsuya Ito · Akira Shimizu · Takashi Nakamura

Received: 6 December 2010 / Revised: 23 January 2011 / Accepted: 16 February 2011

Abstract The objective of this study was to establish the efficacy and safety of porous bioactive titanium metal for use in a spinal fusion device, based on a prospective human clinical trial. A high-strength spinal interbody fusion device was manufactured from porous titanium metal. A bioactive surface was produced by simple chemical and thermal treatment. Five patients with unstable lumbar spine disease were treated surgically using this device in a clinical trial approved by our Ethics Review Committee and the University Hospital Medical Information Network. Clinical and radiological results were reported at the minimum follow-up period of 1 year. The optimal mechanical strength and interconnected structure of the porous titanium metal were adjusted for the device. The whole surface of porous titanium metal was treated uniformly and its bioactive ability was confirmed before clinical use. Successful bony union was achieved in all cases within 6 months without the need for autologous iliac crest bone grafting. Two specific findings including an anchoring effect and gap filling were evident radiologically. All clinical parameters improved significantly after the operation and no adverse effects were encountered during the follow-up period. Although a larger and longer-term follow-up clinical study is mandatory to reach any firm conclusions, the study results show that this porous bioactive titanium metal is promising material for a spinal fusion device.

Keywords Porous titanium metal · Spinal fusion · Biomaterial · Clinical trial

S. Fujibayashi (✉) · M. Takemoto · M. Neo · T. Nakamura
Department of Orthopedic Surgery,
Graduate School of Medicine, Kyoto University,
Kyoto 606-8507, Japan
e-mail: shfuji@kuhp.kyoto-u.ac.jp

T. Matsushita · T. Kokubo
Department of Biomedical Sciences, College of Life and Health Sciences, Chubu University, Kasugai 487-8501, Japan

K. Doi
Osaka Yakin Kogyou Co.,Ltd, Miki 673-0043, Japan

T. Ito · A. Shimizu
Department of Experimental Therapeutics,
Translational Research Center,
Kyoto University Hospital, Kyoto 606-8507, Japan

Introduction

Osteoconductive synthetic materials including sintered hydroxyapatite ($Ca_{10}(PO_4)_6(OH)_2$ or HA), Na_2O-CaO-SiO_2-P_2O_5 system (Bioglass®) and glass ceramics containing apatite and wollastonite (AW-GC) are widely used clinically as bone substitutes [7, 12, 16]. Because application for load-bearing conditions such as the spine or long bones requires high mechanical strength, solid materials are usually used. However, such materials are brittle against shearing forces and bond to the surrounding bone only at their surface. Porous materials have advantages over solid materials in terms of bone bonding, because they can demonstrate both osteoconductive bonding and mechanical interlocking through bone tissue ingrowth into the pores. Conventional porous synthetic materials such as granules of HA and AW-GC have been applied clinically as bone graft expanders for lumbar posterolateral fusion or bone void fillers after tumor excision [8]. However, because of their poor mechanical strength, porous body of such materials cannot be applied in load-bearing conditions. Thus, achieving both high bone-bonding ability and high mechanical strength is quite difficult for porous

Published online: 03 March 2011

materials. To overcome this problem, we have developed porous bioactive titanium metal, which possesses both high bone-bonding ability and high mechanical strength simultaneously [24]. Titanium metal and its alloys can be changed to bioactive materials by simple chemical and thermal surface treatment [9, 18]. This can be applied to porous titanium metal as well [15]. Several experiments on animal models showed the safety and efficacy of porous bioactive titanium metal as a synthetic bone under load-bearing conditions. Our preclinical study [26] demonstrated that bioactive treatment effectively enhanced the fusion ability of the porous titanium implants in a canine model of spinal interbody fusion.

Instrumented spinal fusion with autologous iliac crest bone grafting (ICBG) is a gold-standard surgical procedure for the treatment of unstable spinal diseases. However, grafts harvested from the iliac crest are still a major source of autologous bone and the harvesting process is associated with graft site morbidities including residual pain, long operative times and significant blood loss [1].

To accelerate the fusion rate and alleviate donor site problems, several effective osteoinductive agents including recombinant human bone morphogenetic protein-2 (rhBMP-2) and osteogenic protein-1 (OP-1/BMP-7) have been introduced and are widely used clinically [3, 20]. Excellent clinical results have been documented, although some serious adverse effects (AEs) have been reported such as osteolysis around the cage implant, massive bleeding and soft tissue swelling [19, 27, 31]. Porous bioactive titanium metal is not only osteoconductive but also has osteoinductive ability without the need for additional osteogenic cells or agents [10, 25]. Although the osteoinductive ability of porous bioactive titanium metal is limited and the actual mechanism has not been clarified, the osteogenesis it induces is believed to guarantee the high osteoconductive ability of this material.

We conducted a clinical trial of porous bioactive titanium metal for lumbar interbody fusion. Here, we report our preliminary results and discuss the safety and efficacy of porous bioactive titanium metal as one of a new generation of synthetic device materials. This trial was based upon extensive experiments in animal models and clinical success in cementless total hip prosthesis using porous bioactive titanium metal [14, 26].

Methods

Preparation of porous implants

Porous titanium metal was manufactured from a mixture of commercially pure titanium powder <45 μm in particle size (Osaka Titanium Tech. Co. Ltd, Osaka, Japan) and ammonium hydrogen carbonate as spacer particle [32]. Sintering was carried out at 1,400°C for 2 h in Argon gas. Three types of implants, 7, 8 and 9 mm thick and 30 mm wide, were prepared for the clinical trial (Fig. 1). To improve the safety of handling during surgery, a thin outer frame was placed around the porous body and sintered. These implants were supplied by Osaka Yakin Co. (Osaka, Japan). Micro-computed tomography (CT) analysis demonstrated that more than 99% of the porous structures were interconnected and more than 80% of pores were connected through channels more than 52 μm in diameter (Fig. 2). The average porosity was 60% and the average pore size was 250 μm.

Mechanical properties of the porous titanium implants

The compressive strength of the porous titanium body was measured using a universal testing machine (Model EHF-LV020K1-010, Shimadzu Corp., Kyoto, Japan) at a cross-head speed of 1 mm/min. 0.2% yield compressive strength and Young's modulus of a typical 60% porous body were

Fig. 1 Photograph of porous bioactive titanium device for transforaminal lumbar interbody fusion

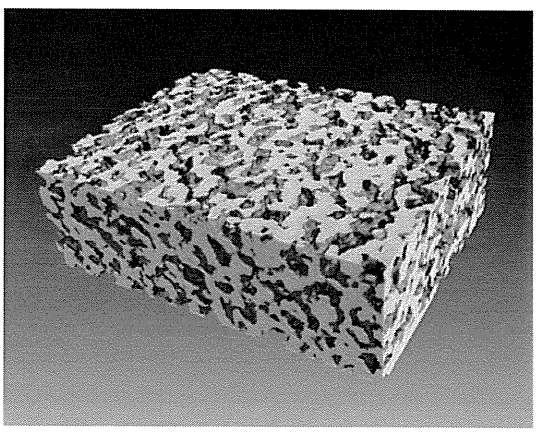

Fig. 2 Micro-computed tomography image showing well-connected internal porous structures

53.0 MPa and 4.2 GPa, respectively. The stiffness was 91.5 kN/m, and this increased to 458.3 kN/m at the outer frame. The porous body combined with the outer frame proved stable against a cyclic load of 10,000 N at 4 Hz for 1,000,000 cycles.

Bioactive surface treatment

The porous implants were treated chemically and thermally to give them a bioactive surface, as described [9, 18]. Briefly, the sintered porous titanium bodies were immersed in 5 M aqueous NaOH solution at 60°C for 24 h, 0.5 mM HCl at 40°C for 24 h, ultrapure water at 40°C for 24 h and then heat-treated at 600°C for 1 h. The homogeneity of the bioactive surface was confirmed by examining the topography and the chemistry of the center and the peripheral parts of several implants using a field emission scanning electron microscope (FE-SEM; Hitachi S-4300, Ibaraki, Japan), an energy-dispersive X-ray microanalyzer (EDX) and X-ray diffractometry (XRD). In vitro apatite-forming ability was confirmed by soaking samples for 3 days in an acellular simulated body fluid (SBF) with ion concentrations (in mM) of Na^+ 142.0, K^+ 5.0, Mg^{2+} 1.5, Ca^{2+} 2.5, Cl^- 147.8, HCO_3^- 4.2, HPO_4^{2-} 1.0 and SO_4^{2-} 0.5: nearly equal to those of human blood plasma at 36.5°C and prerequisite conditions for generating bioactive materials [17]. The implants were sterilized by 25 kGy γ-radiology exposure before surgical implantation.

Evaluation of implants

All devices with the same lot number destined for clinical use were analyzed in vitro before implantation. All parameters of mechanical strength including yield compressive strength, elastic modulus and fatigue strength were within an error of <5%. Mechanical testing found no failure of the device, nor any loss of titanium particles. FE-SEM, EDX and XRD studies confirmed the homogeneity of the bioactive surface both centrally and peripherally. After the surface treatment, the whole porous surface was uniformly changed to a bioactive thin TiO2 layer approximately 1 μm thick with sub-micron-sized pores. The walls of the porous body were completely covered with apatite within 3 days of soaking in SBF, indicating that the whole surface of the implant could be rendered bioactive by the chemical and thermal treatments (Fig. 3a–c).

Transforaminal lumbar interbody fusion (TLIF) [11]

All surgical procedures were performed by the two senior authors (S.F. and M.T.).

Following a midline skin incision, the lateral aspect of facet joints was exposed through a midline subperiosteal approach or Wiltse's approach depending on the case. After bilateral pedicle screw placement, the neural foramen was exposed by excision of the ipsilateral facet joint. Disc space preparation with the removal of degenerative disc materials and cartilaginous endplate was performed carefully from the safety triangle zone between the exiting and traversing nerve roots. In the case of concomitant spinal canal stenosis, neural decompression was done using a surgical microscope. The bioactive porous titanium implant was placed into the intervertebral space through the opened safety triangle zone and small local bone chips were packed around the implant as monitoring bone material. Compressive force was applied through the pedicle screws and pre-bent rods were set on the screws bilaterally. The patients were allowed to walk while wearing a hard brace beginning on the first day after surgery.

Patients

This was a prospective clinical case series on five patients (3 men and 2 women) with degenerative unstable lumbar

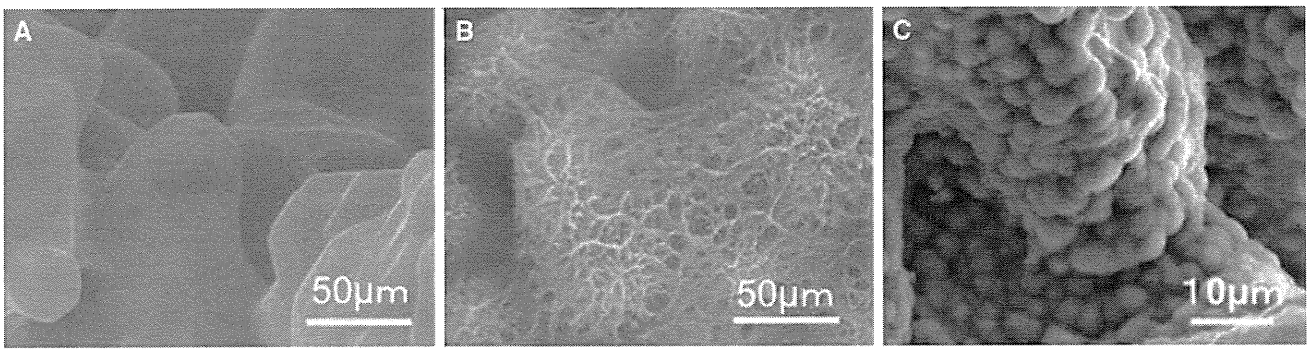

Fig. 3 Field emission scanning electron microscope (FE-SEM) images showing surface morphological changes to the porous titanium metal. **a** Before treatment, the surface was smooth. **b** After chemical and thermal treatment, a thin submicron-sized pore layer was formed on the surface. **c** Apatite formation on the whole surface of the porous bioactive titanium metal after soaking in simulated body fluid (SBF) for 3 days

lesion who were eligible for surgical treatment and who were referred to our University Hospital from November 2008 to June 2009. In all cases, the patient and his or her relatives were informed about the benefits and the risks of the implant. Written informed consent was obtained from all patients and/or their relatives, in accordance with protocols approved by our Institutional Ethics Committee and in agreement with the Declaration of Helsinki.

Among the five patients enrolled there were three with degenerative spondylolisthesis and two with isthmic spondylolisthesis. Inclusion criteria for this preliminary clinical trial were symptomatic single-level unstable lumbar disc disease with or without compression of neural elements, which were refractory to adequate conservative treatments for at least 3 months preoperatively. Patients with multilevel diseases, a previously operated spine, osteoporosis, general inflammatory disease or a severe comorbidity such as cardiovascular disease or renal dysfunction were excluded. The average age of the enrolled patients at surgery was 51.6 years (range 36–61 years).

Clinical assessment

A patient self-assessed 100 mm visual analog scale (VAS) (0 mm = no pain, 100 mm = worst pain imaginable) for both low back pain (LBP) and leg pain (LP), the Japanese Orthopaedic Association (JOA) score (Table 1) and its recovery rate [recovery rate = postoperative score − preoperative score/29 (full score) − preoperative score × 100 (%)] were examined before operation and postoperatively. A self-assessed patient's satisfaction score was examined after the surgery. For subjective assessment of the overall results of surgery, the patient was asked to select from among the options: very satisfied, satisfied, somewhat satisfied, somewhat dissatisfied or dissatisfied. The satisfaction score was recorded as a score at all time points. All patients complained of LBP preoperatively and four complained of concomitant LP. The average preoperative JOA score was 15.8 (range 11–21). The average preoperative VAS values for LBP and LP were 37.6 mm (range 10–50 mm) and 21.4 mm (range 0–60 mm), respectively. An independent expert nurse carried out the assessment of pre- and postoperative VAS and the patient's satisfaction score. The JOA scores and VAS measures were analyzed statistically using paired *t*-tests and $P < 0.05$ was considered statistically significant.

Radiological assessment

Magnetic resonance imaging (MRI), multidetector-row computed tomography (MDCT) and lateral dynamic X-rays were used to assess the neural compression and

Table 1 JOA score classifications for low-back pain

Parameter	JOA score
Subjective symptoms	9
Low-back pain	
None	3
Occasional mild pain	2
Frequent mild or occasional severe pain	1
Frequent or continuous severe pain	0
Leg pain and/or tingling	
None	3
Occasional slight symptoms	2
Frequent slight or occasional severe symptoms	1
Frequent or continuous severe symptoms	0
Gait	
Normal	3
Able to walk >500 m, although it causes pain, tingling, and/or muscle weakness	2
Unable to walk >500 m due to leg pain, tingling, and/or muscle weakness	1
Unable to walk >100 m due to leg pain, tingling, and/or muscle weakness	0
Clinical signs	6
Straight leg-raising test (including tight hamstrings)	
Normal	2
30–70°	1
<30°	0
Sensory disturbance	
None	2
Slight disturbance (not subjective)	1
Marked disturbance	0
Motor disturbance	
Normal (Grade 5/5)	2
Slight weakness (Grade 4/5)	1
Marked weakness (Garde 0–3/5)	0
Restriction of ADL	14
ADL (restriction)	
Turning over while lying down	
Standing	
Washing	
Leaning forward	
Sitting (~1 h)	
Lifting/holding heavy objects	
Walking	
Urinary bladder function	−6
Normal	0
Mild dysuria	−3
Severe dysuria (incontinence, urinary retention)	−6

JOA Japanese Orthopaedic Association

ADL activities of daily living

For each activity of daily living category severe restriction was accorded a score of 0; moderate restriction, a score of 1; and no restriction, a score of 2

dynamic situation. Preoperative dynamic lateral X-rays showed marked segmental instability in all five patients. To assess bony union postoperatively, lateral dynamic radiographs were obtained at 3, 6 and 12 months. More than 3° motion on flexion–extension was considered to indicate nonunion. In addition, radiolucent regions around the pedicle screws and the implant were defined as showing nonunion. To evaluate the placement of implant and pedicle screws, bony union and AEs, coronal and sagittal reconstruction views using MDCT were assessed at 1 week and at 1, 3, 6 and 12 months after surgery. Bony union was defined as complete when there was osseous continuity between bony endplate and implant on both the coronal and sagittal MDCT images. Nonunion was defined as the presence of a visible gap between the vertebral endplate and implant, or radiolucency around the pedicle screws. Successful bony union was recorded when the assessments of aforementioned radiological parameters were complete. A change of 3 mm or more of implant migration into the vertebral endplate was defined as significant subsidence. MRI was performed at 1 week and at 1, 3, 6 and 12 months after surgery to assess neural decompression and dural tube extension, any AEs including inflammatory reaction around the implant such as vertebral endplate erosion, Modic change [20] and any fluid collection. Three independent experienced spinal surgeons, each with at least 10 years of experience, did all the radiological assessments. Each patient's preoperative clinical and radiological data are summarized in Table 2.

Ethical considerations

The study was performed in accordance with the principles of the Declaration of Helsinki and of Good Clinical Practice and was registered on the University Hospital Medical Information Network Clinical Trials Registry (UMIN00000 1448). Approval was obtained from the relevant competent authorities and our institutional Committee of Ethics before the trial began. As clinicians, the authors played a leading role in this new type of clinical trial, which is extremely rare in the development of new medical devices in Japan. We prepared all the protocols of this study by ourselves and were supported by a translational research center in Kyoto University. The independent clinical research coordinator of the translational research center managed all clinical data, which were extracted from each patient's clinical research form. The endpoints of this clinical trial were achievement of good clinical results, bony union, no serious AEs and avoidance of the need for autologous ICBG.

Results

Clinical results

In all five patients, the preoperative LBP and radicular symptoms were resolved immediately after the operation. No surgery-related neurological deficit or wound breakdown was observed in any patient. The mean operating time was 164.6 min (range 154–179 min) and the mean estimated intraoperative blood loss was 192 mL (range 80–310 mL). No patient required transfusion or ICBG. No surgery-related complication was observed. The mean follow-up period was 15.2 months (range 12–19 months). The average postoperative JOA score was 25.6 at 1 month, 25.6 at 3 months, 27 at 6 months and 26.6 at 12 months (range 18–29). The mean recovery rate of the JOA score was 76.6% at 1 month, 77.5% at 3 months, 88.0% at 6 months and 85.8% at 12 months (range 38.9–100%). The postoperative JOA score improved significantly compared with the preoperative score at all times ($P = 0.002$ at 12 months). The mean VAS was 2 mm at 1 month, 2 mm at 3 months, 6 mm at 6 months and 2 mm at 12 months (range 0–30 mm) for LBP. It was 0 mm at 1 month, 0 mm at 3 months, 4 mm at 6 months and 2 mm at 12 months (range 0–20 mm) for LP. Both VAS measures were significantly improved compared with preoperative scores at all times (at 12 months; LBP $P = 0.027$; LP $P = 0.012$). All but one patient satisfied very much through the experiment periods. All clinical parameters showed rapid recovery within 1 month, which indicated a low level of invasiveness and good stabilization of the surgery (Fig. 4).

Table 2 Summary of preoperative patient's demographic data

Case	Age	Sex	Diagnosis	Level	Symptoms	Pre JOA	Pre VAS (LBP)	Pre VAS (LP)
1	54	F	DS	L4/5	LBP + LP	21	10	60
2	36	M	IS	L5/S	LBP + LP	12	80	50
3	51	F	DS	L4/5	LBP	19	80	0
4	61	F	DS	L4/5	LBP + LP	11	60	60
5	56	M	IS	L5/S	LBP + LP	16	50	20

DS degenerative spondylolisthesis, *IS* isthmic spondylolisthesis, *LP* leg pain, *LBP* low back pain, *VAS* visual analog scale

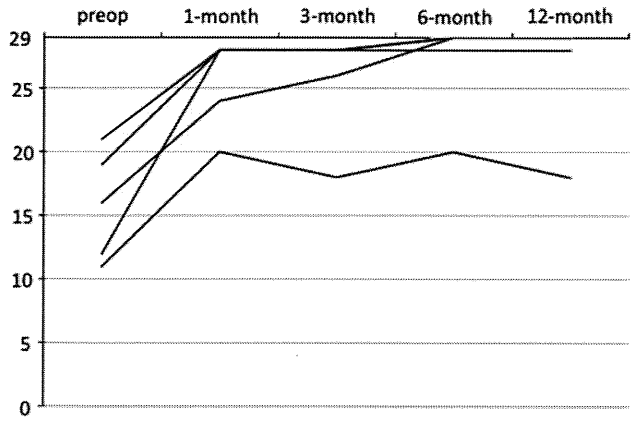

Fig. 4 Sequential changes in the Japan Orthopaedic Association (JOA) score of the five cases. The graph indicates a rapid recovery of the patients' clinical status within 1 month

Radiological results

Dynamic radiological examination showed a solid bony construct without abnormal segmental motion or radiolucency around the implants in all cases after 3 months. No patient exhibited significant implant subsidence during the follow-up period. Immediate postoperative MDCT demonstrated good apposition between the vertebral endplate and implant in all but one case. These findings indicated good anchoring of the porous titanium implant to the surrounding bone. Follow-up MDCT showed good bone ingrown onto the surface of the porous titanium metal without radiolucent line. It also showed remodeling not only of the monitoring bone but also of the surrounding vertebral bone. However, in Case 5, a gap was evident between porous titanium metal and surrounding vertebral endplate on the MDCT image immediately after the operation, because of a poor fit of the device surface with an irregular vertebral endplate. The gap was filled gradually and closed at the final follow-up MDCT (Fig. 5a–c). Because the radiological parameters mentioned above were complete in all cases, bony union was considered to be achieved in all cases by 6 months after the operation. Postoperative MRI scans showed no significant AE such as abnormal fluid collection or apparent change in the Modic sign. In three patients with concomitant spinal canal stenosis, successful neural tissue decompression was also confirmed. The postoperative clinical and radiological results are summarized in Table 3.

Illustrative case (Case 1)

This 54-year-old woman had complained of LBP and intractable bilateral LP for 3 years before surgery. These were refractory to adequate conservative treatment. She also complained of an inability to walk for longer than 10 min, with intermittent claudication. A physical examination demonstrated bilateral dysesthesia on the L5 sensory dermatome. Her preoperative JOA score was 21 points and her self-reported VAS was 10 mm for LBP and 60 mm for LP. X-ray images showed degenerative spondylolisthesis at the L4–5 level with instability (Fig. 6a). Preoperative MR imaging demonstrated severe spinal canal stenosis at the L4–5 level. Transforaminal lumbar interbody fusion and spinal canal decompression using our bioactive titanium was performed. The operating time was 173 min and the estimated intraoperative blood loss was 140 mL. Immediate postoperative coronal imaging using MDCT demonstrated a press fit at the interface between the porous titanium metal and the vertebral endplate (Fig. 6b). Three months after the operation, dynamic X-ray imaging demonstrated no abnormal movement (Fig. 6c). Sagittal imaging using MDCT showed a stable interface without a radiolucent line or any clear zones around the pedicle screws, indicating a successful bony union (Fig. 6d). Postoperative MR imaging showed good neural decompression without any AEs. Her JOA score recovered to 29

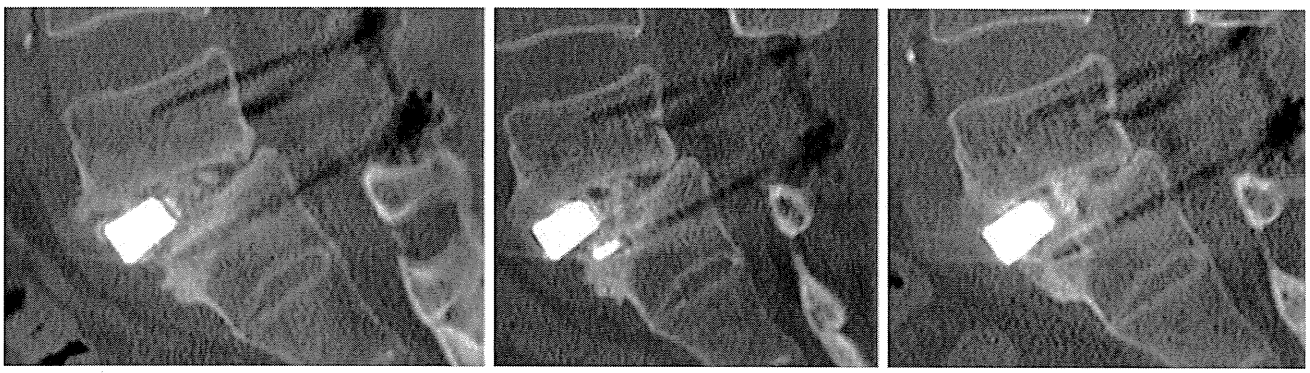

Fig. 5 Sagittal multidetector-row computed tomography (MDCT) images taken immediately postoperatively and at 3 and 12 months for Case 5. The immediate postoperative image (*left*) shows an apparent gap between the porous titanium metal and vertebral bone. The 3-month image (*center*) demonstrates bone ingrowth cranial to the porous titanium metal. The 12-month image (*right*) demonstrates complete gap filling and direct bone bonding to the porous titanium metal

Table 3 Summary of postoperative patient's demographic data

Case	Op. time (min.)	Blood loss (mL)	Post JOA score	JOA score recovery rate (%)	Post VAS (LBP)	Post VAS (LP)	Satisfaction score	ICBG	AEs	Bony union (month)
1	173	140	29	100	0	0	1	–	–	3
2	179	310	29	100	0	0	1	–	–	3
3	160	80	28	90	0	0	1	–	–	3
4	154	228	18	38.9	10	10	4	–	–	6
5	157	192	29	100	0	0	1	–	–	3

ICBG Iliac crest bone graft, *AEs* adverse effects

Satisfaction score 1, very satisfied 2, satisfied 3, somewhat satisfied 4, somewhat dissatisfied 5, dissatisfied

JOA score, VAS, and satisfaction score are obtained at 12 months after the surgery

points and the VAS score was 0 mm for LBP and 0 mm for LP at the final follow-up.

Discussion

Here, we report the safety and efficacy of porous bioactive titanium metal for the treatment of unstable lumbar disc disease. All cases showed early bony union by 6 months without autologous ICBG and rapid recovery after the surgery. The patients' satisfaction and clinical recovery rates were both acceptable.

The use of an interbody fusion cage with autologous bone grafting is a standard procedure for lumbar spinal fusion. However, nonunion, cage subsidence, implant failure and donor site morbidity are still of concern [1]. Porous materials with adequate pore structure and appropriate mechanical properties might represent an alternative to traditional cage implants. Interconnected pores permit tissue ingrowth and thus anchor the prosthesis to the surrounding bone, preventing loosening. This concept also allows a larger support area because no graft space is required and it might be effective for the prevention of implant subsidence. In the current study, significant implant subsidence has not occurred throughout the follow-up periods. Furthermore, if bone bridging can be achieved across the whole implant through the interconnected pores from one vertebra to the other it reduces the risk of implant failure and ensures long-term stability.

The kind of material and its pore characteristics influence the mechanical strength of porous biomaterials. Porous HA implants have good biocompatibility and osteoconductivity, but their mechanical properties are not adequate for load-bearing conditions. The clinical application of such conventional porous materials is limited to non-load-bearing conditions. Therefore, the use of metal to produce porous implants with higher mechanical strength is required. By using titanium metal as a starting material, our device with high porosity and large pore size acquired a high mechanical strength that is adequate for load-bearing conditions. In a previous study, we investigated the relationship between pore structure and bone ingrowth in vivo using several types of porous titanium implants. We concluded that not only high porosity and large pore size but also high interconnectivity of the pores is effective for bone ingrowth and tissue differentiation [23]. Based on this previous study, an optimally structured porous titanium metal was developed and used for this clinical trial. It has 60% porosity, 250 μm average pore size and more than 99% pore interconnectivity.

Another important issue associated with porous metal implants is the difficulty in producing bioactive properties on the inner surfaces of implants using conventional methods such as applying a plasma-sprayed HA coating. In the absence of a bioactive surface, the osteoconductivity of these implants and their capacity to promote fusion is limited. The thickness of a conventional HA coating layer is about 40–50 μm, which cannot be applied to critical supporting structures without changes to surface morphology [5]. Moreover, the conventional HA coating for titanium metal implants has the potential for degradation, absorption and third body wear during long-term implantation, which might be related to its poor clinical results [2, 21]. Our chemical and thermal treatments ensured that bioactive properties were applied to the whole surface of the porous titanium implants without reducing the pore space available for bone ingrowth [15]. Adequate stability of the thin treated layer was confirmed both in vitro and in vivo and might assure the long-term apposition with surrounding bone [9]. This material also offers sufficient resistance to shearing forces during the implantation of treated cementless hip prostheses.

Although titanium metal and its alloys are 'gold standard' materials in orthopedics, one of the potential disadvantages of a metal device is a high elastic modulus. The elastic modulus of solid titanium metal is more than 100 GPa and this will lead to stress shielding around the metal device during long-term implantation. To reduce such a mechanical mismatch between the implant and host

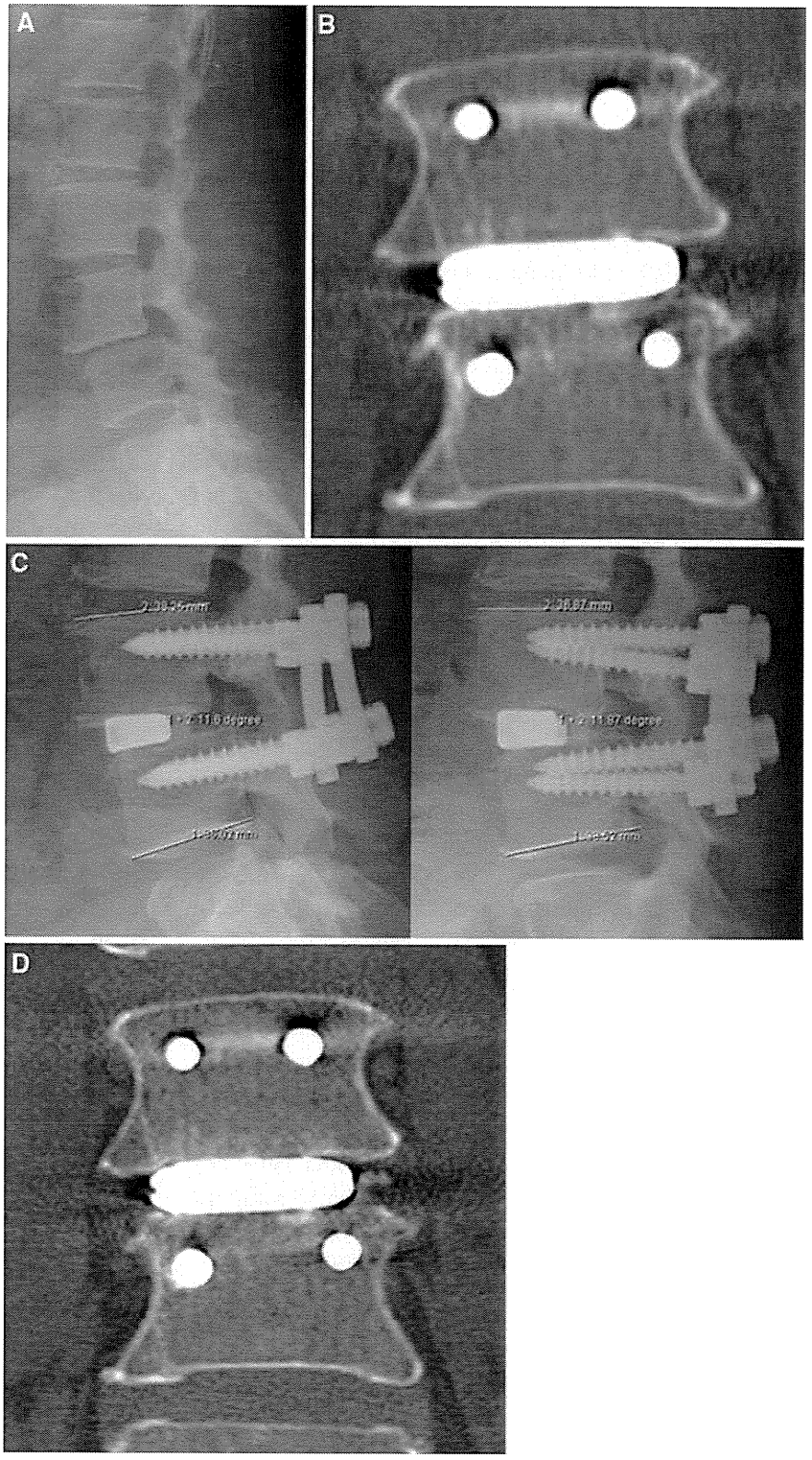

Fig. 6 Preoperative and postoperative radiological studies obtained from a 54-year-old woman with degenerative spondylolisthesis at L4–5 (Case 1). **a** Plain lateral X-ray demonstrating L4 listhesis. **b** Immediate postoperative MDCT image demonstrating a press fit of the porous titanium metal implant to the vertebral endplate. **c** Dynamic lateral radiographs at 3 months showing a solid construct without abnormal segmental motion (*left* flexion; *right* extension). **d** Coronal MDCT image demonstrating solid bony union without device subsidence or any radiolucency at 3 months after surgery

bone, several types of soft material including polyetheretherketone and carbon have been introduced clinically [6, 28]. Although there are no long-term results as yet, porous titanium metal will reduce stress shielding, because the elastic modulus of this material with 60% porosity is 4.2 GPa, close to the value of human cortical bone and much less than solid metal materials. According to Nachemson's study, loads to the human lumbar spine are between 1,000 and 3,000 N during most everyday activities, and increases in different body positions give possible values in excess of 3,000 N during significant lifting [22]. Based upon these data, Brantigan suggested that a lumbar

interbody fusion construct must bear an immediate postoperative load at the bone-implant interface of at least 2,400 N during activities of daily living [4]. On the other hand, breakage of the carbon cage and dissemination of free carbon particles occurred in one case of implant nonunion [29]. A biomechanical study revealed that the carbon cage fractures at around 5,800–8,800 N and concluded that at least 5,000 N was required for an interbody fusion cage [13]. The fatigue strength of porous titanium metal combined with an outer frame is more than 10,000 N under a repetitive compressive load, so it can be used as a spinal interbody fusion device safely.

Another potential disadvantage of a pure metal device is the difficulty of confirming fusion status radiologically because of its high radiodensity. Usually, bony union is confirmed when the following radiological parameters are complete: visible continuous grafted bone trabeculation, no abnormal movement on dynamic study and no radiolucency around the implants. In the case of metal devices such as a titanium cage, bone trabeculation through the cage is difficult to identify on plain X-ray images. However, definitive diagnoses of bony union have become easier with the introduction of MDCT, especially in the case of porous titanium metal, because the metal content is less than with the solid form, recognition of fusion status such as bone-implant interface and bony trabeculation around the implant is not so difficult on MDCT images. In the current study, two specific radiological findings were evident. The first of these was the anchoring effect between the porous bioactive titanium implant and the surrounding vertebral endplate seen on the images taken immediately after surgery. This could be attributed to the optimally rough surface of the porous bioactive device. The second finding was the gap-filling effect. The radiological evidence of gap filling as shown in Fig. 6 resembles the results of alkali- and heat-treated total hip prostheses. Radiological gaps between alkali- and heat-treated metal shells and the acetabulum were filled within 1 year, which indicated the high osteoconductive ability of bioactive titanium metal [14]. The best feature of porous bioactive titanium metal is that it permits bone ingrowth through the inner pore structure. Although we reported good bone ingrowth to the pores in several studies using animal models, we could not confirm this evidence using noninvasive radiological examinations in the present study.

There are some limitations to this study, including its small sample size, short follow-up period and preliminary nature. Our chemical and thermal treatment has been applied clinically for cementless total hip prostheses after a strict clinical trial, which was approved by the Ministry of Health, Labor and Welfare in Japan. Excellent mid-term (4.8 years) clinical results and early bone apposition were reported [14]. These results are encouraging for the efficacy and safety of this surface treatment on titanium and its alloys. Moreover, TLIF is a promising standard procedure for the treatment of patients with unstable spinal disease. Given these encouraging results, we planned this small clinical trial as much as possible to test the efficacy and safety of porous bioactive titanium metal in a spinal fusion device. Fortunately, there was successful bony union without the need for autologous ICBG in this small series. However, implantation of metal devices has a potency to bring about several late complications such as stress shielding and adjacent segment disease during long-term implantation. Therefore, long-term clinical results are mandatory to reveal the true efficacy and safety of this device.

We consider that porous bioactive titanium metal is superior to other porous metal materials in terms of safety, osteoconductive and osteoinductive abilities, mechanical strength and controllable optimum microstructure [10, 24]. Another advantage of porous bioactive titanium metal is its potency for general purpose medical devices. First, our surface treatment can be applied not only to pure titanium but also to several types of titanium alloys. By changing materials, the mechanical characteristics can be optimized. Second, using our manufacturing technique, the pore structure, mechanical strength and biological characteristics can be controlled depending on the conditions. This material will be valuable not only for spinal fusion but also for reconstructive surgery to the skull, the maxillofacial region and in other orthopedic fields. Moreover, adjustments to the elastic modulus and bioactive abilities promise to produce new generations of devices for the treatment of osteoporotic bone.

Conclusions

We developed porous bioactive titanium device for spinal fusion. The optimal mechanical strength and interconnected structure of porous titanium metal were adjusted to the device. The whole surface of porous titanium was treated chemically and thermally to form the bioactive surface. Clinical trial was successfully performed and early bony union was achieved in all cases without ICBG by 6 months. Two specific findings including an anchoring effect and gap filling were evident radiologically. Although a larger and longer-term follow-up clinical study is mandatory to reach any firm conclusions, we consider this porous bioactive titanium metal is promising material for a spinal fusion device.

Acknowledgments The authors thank Hisashi Kitagaki, Tsuneo Teraoka, of Osaka Yakin Co., for manufacturing and providing the porous titanium implants. They thank Seiji Yamaguchi, of Chubu University Biomedical Sciences, for treating the material chemically.

They thank Shuji Higuchi, Masanori Fukushima, Satoshi Teramukai, Kenichi Yoshimura, Toshinori Murayama, Tomoko Yokota, Erika Hirata and Harue Tada, of Kyoto University's translational research center, for help in protocol preparation, moderation of the clinical trial and data management. They also thank Takeshi Sakamoto, Makoto Yoshida and Masahiko Miyata for radiological assessments, and Masato Ota for surgical assistance.

This study was supported by a Grant in Aid for Scientific Research from the Japan Society for the Promotion of Science (No. 19200039). No benefits in any form have been or will be received from a commercial party related directly or indirectly to the subject of this manuscript. This manuscript has not been previously published and is not under consideration for publication elsewhere. The first two authors contributed equally to this study and preparation of this manuscript.

References

1. Banwart JC, Asher MA, Hassanein RS (1995) Iliac crest bone graft harvest donor site morbidity. A statistical evaluation. Spine 20:1055–1060
2. Bloebaum RD, Beeks D, Dorr LD, Savory CG, DuPont J, Hofmann AA (1994) Complications with hydroxyapatite particulate separation in total hip arthroplasty. Clin Orthop 298:19–26
3. Boden SD, Zdeblick TA, Sandu HS, Heim SE (2000) The use of rhBMP-2 in interbody fusion cages: definitive evidence of osteoinduction in humans: a preliminary report. Spine 25:376–381
4. Brantigan JW, Cunningham BW, Warden K, McAfee PC, Steffee AD (1993) Compression strength of donor bone for posterior lumbar interbody fusion. Spine 18:1213–1221
5. De Groot K, Geesink R, Klein CP, Serekian P (1987) Plasma sprayed coatings of hydroxyapatite. J Biomed Mater Res 21: 1375–1381
6. Desogus N, Ennas F, Leuze R et al (2005) Posterior lumbar interbody fusion with PEEK cages: personal experience with 20 patients. J Neurosurg Sci 49:137–141
7. Ducheyne P, Qiu Q (1999) Bioactive ceramics: the effect of surface reactivity on bone formation and bone cell function. Biomaterials 20:2287–2303
8. Fujibayashi S, Shikata J, Tanaka C, Matsushita M, Nakamura T (2001) Lumbar posterolateral fusion with biphasic calcium phosphate ceramic. J Spinal Disord 14:214–221
9. Fujibayashi S, Nakamura T, Nishiguchi S, Tamura J, Uchida M, Kim HM et al (2001) Bioactive titanium: effect of sodium removal on the bone-bonding ability of bioactive titanium prepared by alkali and heat treatment. J Biomed Mater Res 56:562–570
10. Fujibayashi S, Neo M, Kim HM, Kokubo T, Nakamura T (2004) Osteoinduction of porous bioactive titanium metal. Biomaterials 25:443–450
11. Fujibayashi S, Neo M, Takemoto M, Ota M, Nakamura T (2010) Paraspinal-approach transforaminal lumbar interbody fusion for the treatment of lumbar foraminal stenosis. J Neurosurg Spine 13:500–508
12. Hench LL (1998) Bioactive materials: the potential for tissue regeneration. J Biomed Mater Res 41:511–518
13. Jost B, Cripton PA, Lund T, Oxland TR, Lippuner K, Jaeger P et al (1998) Compressive strength of interbody cages in lumbar spine: the effect of cage shape, posterior instrumentation and bone density. Eur Spine J 7:132–141
14. Kawanabe K, Ise K, Goto K, Akiyama H, Nakamura T, Kaneuji A et al (2009) A new cementless total hip arthroplasty with bioactive titanium porous-coating by alkaline and heat treatment: average 4.8-year results. J Biomed Mater Res Part B: Appl Biomater 90B:476–481
15. Kim HM, Kokubo T, Fujibayashi S, Nishiguchi S, Nakamura T (2000) Bioactive macroporous titanium surface layer on titanium substrate. J Biomed Mater Res 52:553–557
16. Kokubo T (1991) Bioactive glass ceramics: properties and applications. Biomaterials 12:155–163
17. Kokubo T, Kushitani H, Sakka S, Kitsugi T, Yamamuro T (1990) Solutions able to reproduce in vivo surface-structure changes in bioactive glass-ceramic A-W. J Biomed Mater Res 24:721–734
18. Kokubo T, Miyaji F, Kim HM, Nakamura T (1996) Spontaneous formation of bonelike apatite layer on chemically treated titanium metals. J Am Ceram Soc 79:1127–1129
19. McClellan JW, Mulconrey DS, Forbes RJ, Fullmer N (2006) Vertebral bone resorption after transforaminal lumbar interbody fusion with bone morphogenetic protein (rhBMP-2). J Spinal Disord Tech 19:483–486
20. Modic MT, Steinberg PM, Ross JS, Masaryk TJ, Carter JR (1988) Degenerative disk disease: assessment of changes in vertebral body marrow with MR imaging. Radiology 166:193–199
21. Morscher EW, Hefti A, Aebi U (1998) Severe osteolysis after third body wear due to hydroxyapatite particles from acetabular cup coating. J Bone Joint Surg Br 80:267–272
22. Nachemson AL (1981) Disc pressure measurements. Spine 6:93–97
23. Otsuki B, Takemoto M, Fujibayashi S, Neo M, Kokubo T, Nakamura T (2006) Pore throat size and connectivity determine bone and tissue ingrowth into porous implants: three-dimensional micro-CT based structural analyses of porous bioactive titanium implants. Biomaterials 27:5892–5900
24. Takemoto M, Fujibayashi S, Neo M, Suzuki J, Kokubo T, Nakamura T (2005) Mechanical properties and osteoconductivity of porous bioactive titanium. Biomaterials 26:6014–6023
25. Takemoto M, Fujibayashi S, Neo M, Suzuki J, Matsushita T, Kokubo T, Nakamura T (2006) Osteoinductive porous titanium implants: effect of sodium removal by dilute HCl treatment. Biomaterials 27:2682–2691
26. Takemoto M, Fujibayashi S, Neo M, So K, Akiyama N, Matsushita T et al (2007) A porous bioactive titanium implant for spinal interbody fusion: an experimental study using a canine model. J Neurosurg Spine 7:435–443
27. Toth JM, Boden SD, Burkus JK MD, Badura JM, Peckham SM, McKay WF (2009) Short-term osteoclastic activity induced by locally high concentrations of recombinant human bone morphogenetic protein-2 in a cancellous bone environment. Spine 34:539–550
28. Tullberg T, Brandt B, Rydberg J, Fritzell P (1996) Fusion rate after posterior lumbar interbody fusion with carbon fiber implant: 1-year follow-up of 51 patients. Eur Spine J 5:178–182
29. Tullberg T (1998) Failure of a carbon fiber implant: a case report. Spine 23:1804–1806
30. Vaccaro AR, Lawrence JP, Patel T, Katz LD, Anderson DG, Fischgrund JS et al (2008) The safety and efficacy of OP-1 (rhBMP-7) as a replacement for iliac crest autograft in posterolateral lumbar arthrodesis. Spine 33:2850–2862
31. Vaidya R, Sethi A, Bartol S, Jacobson M, Coe C, Craig JG (2008) Complications in the use of rhBMP-2 in PEEK cages for interbody spinal fusions. J Spinal Disord Tech 21:557–562
32. Wen CE, Mabuchi M, Yamada Y, Shimojima K, Chino Y, Asahina T (2001) Processing of biocompatible porous Ti and Mg. Scripta Mater 45:1147–1153

Acta Biomaterialia 7 (2011) 2327–2336

Contents lists available at ScienceDirect

Acta Biomaterialia

journal homepage: www.elsevier.com/locate/actabiomat

Osteoinduction of porous Ti implants with a channel structure fabricated by selective laser melting

A. Fukuda [a,*], M. Takemoto [a], T. Saito [a], S. Fujibayashi [a], M. Neo [a], Deepak K. Pattanayak [b], T. Matsushita [b], K. Sasaki [c], N. Nishida [c], T. Kokubo [b], T. Nakamura [a]

[a] Department of Orthopaedic Surgery, Graduate School of Medicine, Kyoto University, Shogoin, Kawahara-cho 54, Sakyo-ku, Kyoto 606-8507, Japan
[b] Department of Biomedical Sciences, College of Life and Health Sciences, Chubu University, 1200 Matsumoto-cho, Kasugai, Aichi 487-8501, Japan
[c] Sagawa Printing Co. Ltd., 5-3 Inui, Morimoto-cho, Mukou, Kyoto 617-8581, Japan

ARTICLE INFO

Article history:
Received 14 September 2010
Received in revised form 22 January 2011
Accepted 27 January 2011
Available online 2 February 2011

Keywords:
Osteoinduction
Interconnective pore size
Channel structure
Bioactive titanium
Selective laser melting

ABSTRACT

Many studies have shown that certain biomaterials with specific porous structures can induce bone formation in non-osseous sites without the need for osteoinductive biomolecules, however, the mechanisms responsible for this phenomenon (intrinsic osteoinduction of biomaterials) remain unclear. In particular, to our knowledge the type of pore structure suitable for osteoinduction has not been reported in detail. In the present study we investigated the effects of interconnective pore size on osteoinductivity and the bone formation processes during osteoinduction. Selective laser melting was employed to fabricate porous Ti implants (diameter 3.3 mm, length 15 mm) with a channel structure comprising four longitudinal square channels, representing pores, of different diagonal widths, 500, 600, 900, and 1200 μm (termed p500, p600, p900, and p1200, respectively). These were then subjected to chemical and heat treatments to induce bioactivity. Significant osteoinduction was observed in p500 and p600, with the highest observed osteoinduction occurring at 5 mm from the end of the implants. A distance of 5 mm probably provides a favorable balance between blood circulation and fluid movement. Thus, the simple architecture of the implants allowed effective investigation of the influence of the interconnective pore size on osteoinduction, as well as the relationship between bone quantity and its location for different pore sizes.

1. Introduction

Bioactive materials such as bioglass, hydroxyapatite (HA), other calcium phosphate-based biomaterials, and A–W glass ceramic can directly bond to living bones [1] via an apatite layer. Furthermore, when these bioactive materials have a specific porous structure they sometimes become osteoinductive within soft tissues even without the addition of osteogenic cells or bone morphogenetic protein [2–9]. We have previously shown that even porous Ti containing no calcium phosphate can become osteoinductive when it has a complex interconnecting porous structure and bioactive surfaces activated by simple chemical and thermal treatments [10]. In these studies we found that complex macroporous structures, microrough surfaces, and apatite-forming abilities are prerequisites for osteoinduction. Modification of the physico-chemical or surface properties appears to be an attractive method for improving the osteogenic capacity of synthetic materials. Although the clinical utility of osteoinductivity in biomaterials remains controversial, some reports have suggested that this property is a distinct advantage for biomaterials intended for use as bone substitutes [11–14]. Therefore, we believe that it is important in the development of porous biomaterials to tailor osteoinductivity to the specific purpose.

For macroporous structures in general it is recognized that well-defined concavities are important. However, the most suitable pore structure has not been clearly identified. In previous studies we employed plasma sprayed or powder sintered porous bioactive Ti in order to investigate the influence of different porous structures on osteoinduction [10,15]. However, the conventional manufacturing methods employed in our previous studies did not allow precise control over porosity, pore size, and interconnectivity. Furthermore, other osteoinductive materials, such as porous biphasic calcium phosphate [16,17] and porous β-tricalcium phosphate [18,19], are unsuitable for the investigation of macroporous structures because their pore structures change over the implantation period.

Since the 1980s rapid prototyping (RP) technology has emerged as a revolutionary manufacturing process with inherent capabilities for the rapid fabrication of objects of virtually any shape. Using this technology it has become possible to automatically generate three-dimensional (3D) objects by combining computer-aided

* Corresponding author. Tel.: +81 75 751 3365; fax: +81 75 751 8409.
E-mail address: akinobu@kuhp.kyoto-u.ac.jp (A. Fukuda).

1742-7061/$ - see front matter © 2011 Acta Materialia Inc. Published by Elsevier Ltd. All rights reserved.
doi:10.1016/j.actbio.2011.01.037

design (CAD) data and computer-aided manufacturing (CAM), and such objects have been used to fabricate scaffolds or orthopedic implants [20–22]. Furthermore, when Ti is used in RP to produce biomaterials it must be non-resorbable and structurally invariant for accurate evaluation of the pore structure. Among the several RP techniques available we adopted the selective laser melting (SLM) [20–22] process, because it is compatible with Ti and can be used to control the configurations directly with dimensional accuracies of the order of several hundred micrometers. SLM is a powder-based additive manufacturing technique that is capable of producing parts in a layer by layer fashion from a 3D CAD model by employing a high energy laser beam that fuses the metal powders present in its focal zone. SLM is now considered a promising fabrication technique, and we intend to apply it to orthopedic implants under load-bearing conditions.

SLM allows the manufacture of implants with an irregular structure that mimics that of human cancellous bone, which thus far had not been possible with commercially pure Ti (cp-Ti). We reported the tensile strength, surface structure, and apatite forming ability of such devices after chemical and thermal treatment [23]. Furthermore, in our preliminary study these cancellous bone mimicking Ti implants were found to be effective bone substitutes in vivo because of the osteoconductivity and osteoinductivity induced by our chemical and thermal treatments.

In the present study, we evaluated the effects of the interconnective pore size on osteoinductivity (speed, amount, and location of bone formation) to establish basic data for developing a porous osteoinductive biomaterial. At the same time we expect to acquire new knowledge about the mechanisms behind osteoinduction.

For this purpose we used SLM to manufacture porous Ti implants, referred to as channel implants, each with four square longitudinal channels, representing interconnected pores, of different diagonal widths, 500, 600, 900, and 1200 μm. This pore design allowed a comparison of osteoinductivity for different pore sizes in identical environments. These implants were subsequently chemically and thermally treated to induce bioactivity [12] and then implanted into the back muscles of mature beagle dogs.

2. Materials and methods

2.1. Materials

Cylindrical channel implants (diameter 3.3 mm, length 15 mm) were designed using a CAD program (Magics®, Materialise, Belgium) (Fig. 1A) and the design data stored in STL file format, commonly used in stereolithography. All the cylinders had four longitudinal square channels, acting as pores, of different diagonal widths, 500, 600, 900, and 1200 μm. In the present paper these cylinders are referred to as p500, p600, p900, and p1200, respectively. As outlined above, we set this range of target channel sizes on the basis of the fact that an SLM machine can only efficiently produce features larger than 500 μm across and the reported upper limit for osteoconduction is around 1000 μm [24–27]. The STL data were converted into slice data that defined the path for the laser scan inside the cross-sectional contours of the produced shapes. The channel implants were fabricated by an EOSINT M270 SLM machine (Electro Optical Systems GmbH, Germany) using cp-Ti powder (>99.5% pure) with particle diameters of less than 45 μm (Osaka Titanium Technologies, Japan).

2.2. Manufacturing porous Ti implants

After the slice data had been obtained the porous Ti powder was melted using an Yb fiber laser beam in an argon gas atmosphere and then the selected slice of the product was solidified. Then the top of the previously melted surface was recoated with a layer (thickness 30 μm) of fresh Ti powder using a recoater blade. Subsequently, selective irradiation was again carried out using the laser beam. These steps were repeated and as the layers were stacked on top of each other the final geometry was achieved. The process

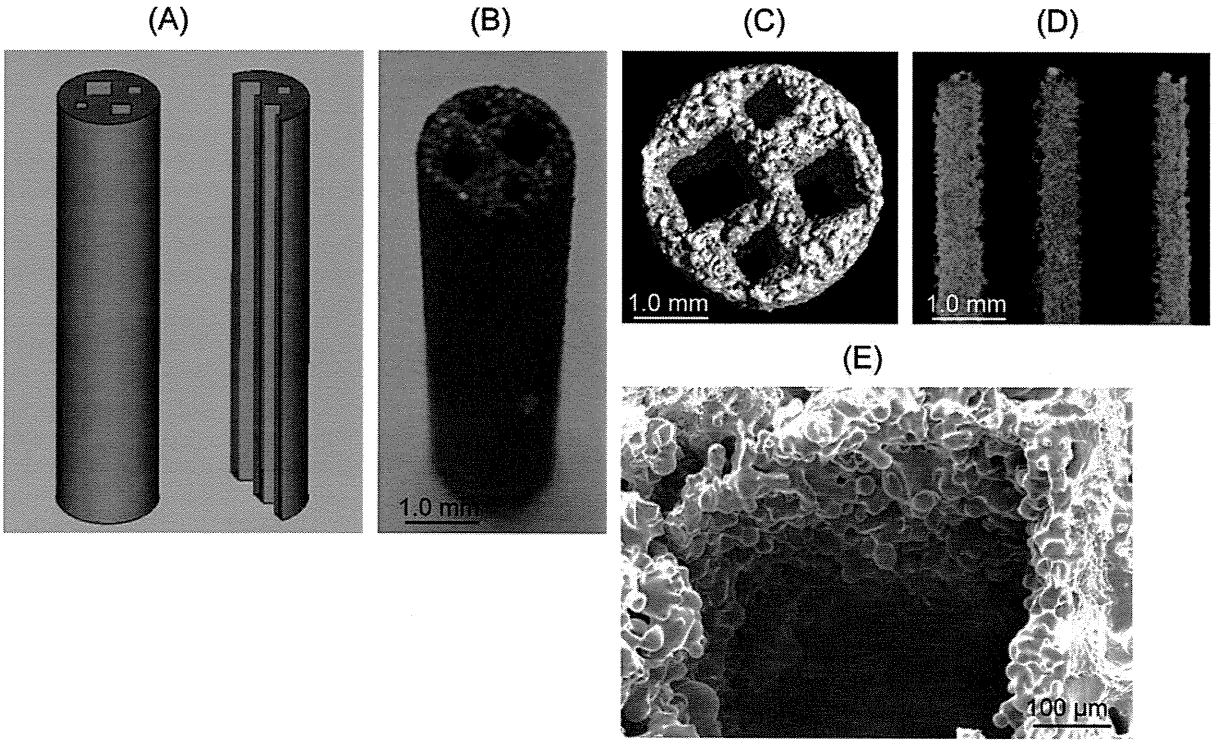

Fig. 1. (A) Computer-aided design (CAD) of a channel implant with four square channels (diagonal widths 500, 600, 900, and 1200 μm). (B) Manufactured channel implant. (C, D) Microcomputed tomography (μCT) of the rapid prototyped channel implant. (E) SEM image of a cross-section of after heat treatment at 1300 °C. Microporous structure was observed on the surface of the smallest of the four pores (500 μm).

parameters for the SLM method were optimized to suppress distortion during the layered fabrication process [28] and were as follows: laser power 117 W, scanning speed 225 mm s^{-1}, hatch spacing 90 μm, hatch offset 20 μm. After the SLM process the channel implants were heat treated at 1300 °C for 1 h and allowed to naturally cool in the furnace under an argon gas atmosphere to enhance ductility and to introduce small cavities on the walls of the channels (Fig. 1B).

2.3. Assessment of manufactured implant structure

About 10 samples were fabricated and the sizes of their various parts measured. Three slices were chosen randomly from each sample and were accurately measured by high resolution X-ray microcomputed tomography (micro-CT) (SMX-100CT-SV3, Shimadzu Co., Japan). The values obtained were averaged. The average values of the outer diameter and shaft length of the implants and the diagonal width of each channel were compared with the design values. The channel implants were also examined under a scanning electron microscope (S-4700, Hitachi Ltd., Japan).

2.4. Induction of bioactivity

The channel implants were soaked in 5.0 M aqueous NaOH at 60 °C for 24 h and then in 0.5 mM HCl (pH 3.4) at 40 °C for 24 h, gently washed with distilled water, and dried at 40 °C for 24 h at room temperature [12]. During these solution treatments the samples were inserted into a polypropylene tube with an inner diameter of 3.6 mm and the solutions were forced into the channels and over the outside surface using a pump. These implants were subsequently heated to 600 °C in an electric furnace at a heating rate of 5 °C min^{-1}, maintained at 600 °C for 1 h, and then allowed to cool to room temperature. Untreated implants were used as control samples.

2.5. Assessment of in vitro apatite forming ability of channel implants

The in vitro apatite forming ability of the channel implants was examined using a simulated body fluid (SBF) having a pH of 7.40 and the ion concentrations (mmol l^{-1}): Na^+ 142.0, K^+ 5.0, Ca^{2+} 2.5, Mg^{2+} 1.5, Cl^- 147.8, HCO_3^- 4.2, HPO_4^{2-} 1.0, SO_4^{2-} 0.5 [29,30]. The channel implants remained in SBF for 3–7 days at 36.5 °C under the reflux conditions mentioned in Section 2.4, then were removed from the SBF, washed with distilled water, and dried on a clean bench. The surface of the samples was examined by field emission scanning electron microscopy (FE-SEM) (S-4300, Hitachi, Japan), and any apatite formed was identified by thin film X-ray diffractometry (TF-XRD) (RINT-2500, Rigaku Co., Japan).

2.6. Animal study

The channel implants were conventionally sterilized using ethylene oxide gas and then implanted in the dorsal muscles of eight mature beagle dogs (weight 10–11 kg), for periods of 16, 26, or 52 weeks. The animals were anesthetized by intramuscular administration of ketamine hydrochloride (50 mg kg^{-1}), followed by diazepam (5 mg) and atropine sulfate (0.5 mg), without endotracheal intubation. Just before the operation a dose of 10 mg kg^{-1} pentobarbital sodium was injected intravenously. During the operation the dogs received an intravenous infusion of saline containing isepamicin sulfate antibiotic. The operations were performed under standard sterile conditions. After incising the skin and fascia, muscle pouches were carefully made in the dorsal muscle to limit any bleeding. Three treated implants and three untreated implants were inserted on both the right and left sides of the dorsal muscles. Each pouch was marked with 3-0 nylon sutures to facilitate explantation. Two implants each were removed from the eight animals under the anesthesia mentioned above at 16, 26, and 52 weeks.

This animal study was approved by the Animal Research Committee, Graduate School of Medicine, Kyoto University, Japan.

2.7. Histological examination

Following killing the implant sites were removed and prepared for histological examination. The specimens were fixed in 10% phosphate-buffered formalin with a pH of 7.25 for 7 days and dehydrated in serial concentrations of ethanol (70, 80, 90, 99, 100, and 100 vol.%) for 3 days each. The specimens were then embedded in polyester resin and cut with a band saw (BS-3000CP, EXACT cutting system, Norderstedt, Germany) perpendicular to the longitudinal axis of the implant from both ends to the mid portion at 1 mm intervals. The sliced samples were ground at their ends to a thickness of 60–70 μm using a grinding–sliding machine (microgrinding MG-4000, EXACT) in order to clarify the distance from the ends of the implants (Fig. 2A). As a result, the mid portion of the channel implants was in the seventh slice, as the total number of slices was 14. For staining we used the method of Maniatopoulos et al. [31], who reported that cells and extracellular structures are stained blue with Stevenel's blue and bone is stained orange or purple with Van Gieson's picrofuchsin. An in-depth microscopic analysis was performed on the histological slides using transmitted light microscopy (Nikon Model Eclipse 80i) in conjunction with a digital camera (Nikon DS-5M-L1).

Several sections were ground with diamond paper until the staining had been removed and a thin layer of carbon was applied for observation by backscattered SEM and SEM energy dispersive X-ray microanalysis (SEM-EDX).

2.8. Histomorphometric examination

Bone formation in each channel was evaluated by light and fluorescence microscopy. The percent bone formation length (PBFL), which is the percentage of slices with bone from among the total 14 slices per implant in each channel, was evaluated for each implantation time (Fig. 2B).

The percent bone formation area (PBFA), which is the percentage of channel area covered with bone in each channel at each distance along the channel, was measured on a personal computer using Adobe Photoshop CS3 and Image J (NIH). The cumulative total bone formation area (i.e. PBFA × channel area, in mm^2) on each slice for each channel was defined as the total induced bone volume (TIBV) (mm^3). We then averaged the PBFA of each slice for each channel (Fig. 2C). Finally, the locations where osteoinduction occurred in each channel were identified. These locations were represented as a line graph of PBFA of each channel at the respective distance from the near end.

2.9. Statistical analysis

Four different channel widths (p500, p600, p900, and p1200) were analyzed for each implantation period (16, 26, and 52 weeks post-implantation). Data was recorded as the mean ± standard deviation (SD) and assessed using one-way analysis of variance (ANOVA) followed by Tukey–Kramer multiple comparison post hoc tests. Differences of $P < 0.05$ were considered to be statistically significant.

3. Results

3.1. In vitro evaluation

3.1.1. Manufacture and characterization of rapid prototyped channel implants

The measured values from the micro-CT images (Fig. 1C and D) for the 10 samples are averaged and summarized in Table 1. The